ELSEVIER

Journal of Magnetism and Magnetic Materials 169 (1997) 289–302

Journal of magnetism and magnetic materials

Synthesis and properties of $Cd_{1-x}Mn_xS$ diluted magnetic semiconductor ultrafine particles

R.J. Bandaranayake, J.Y. Lin, H.X. Jiang, C.M. Sorensen*

Department of Physics, Kansas State University, 116 Cardwelll Hall, Manhattan, KS 66506-2601, USA

Received 18 November 1996; revised 2 December 1996

Abstract

$Cd_{1-x}Mn_xS$ diluted magnetic semiconductor ultrafine particles with sizes in the range 20 to $\sim$ 1200 Å and $0 \leqslant x \leqslant 0.5$ have been synthesized by using aqueous solution precipitation. We find that size has a significant effect on the magnetic spin-glass (SG) properties of these systems. The SG freezing temperature T_f decreases with size, and there is a minimum size below which the SG does not form. The field dependence of T_f and the relaxation of the isothermal remanent magnetization are also significantly different than in the bulk.

PACS: 75.50.Pp; 61.46 + W; 75.50.Lk

Keywords: Diluted magnetic semiconductor; Ultrafine particles; Spin-glass properties

1. Introduction

Diluted magnetic semiconductors (DMS), also known as semimagnetic semiconductors, are a group of materials that have attracted a great deal of attention in the recent past because of their unique properties which promise many potential applications [1–3]. DMS differ from ordinary semiconductors because a fraction of their metallic ions are replaced by some species of magnetic ions. A typical example which has attracted recent interest is magnetic alloys of the type $A^{II}_{1-x}Mn_xB^{VI}$, where A^{II} and B^{VI} represent elements from groups IIB and VIA of the periodic table. The reason Mn^{2+} ions enjoy such wide popularity in forming DMS alloys is threefold. First, Mn^{2+} ions can be incorporated into a $A^{II}B^{VI}$ semiconductor host in large proportions without substantially altering the crystallographic quality of the material. Second, Mn^{2+} has a relatively large magnetic moment ($S = \frac{5}{2}$) due to the $4s^0\ 3d^5$ electronic configuration in its outer shells. Finally, Mn^{2+} is electrically neutral in a $A^{II}B^{VI}$ host, thus avoiding the formation of any acceptor or donor impurities in the crystal. Typical examples of these DMS

* Corresponding author. Tel.: + 1-913-532-6786; fax: + 1-913-532-6806.

0304-8853/97/$17.00
PII S0304-8853(96)00746-9

alloys include $Cd_{1-x}Mn_xSe$, $Zn_{1-x}Mn_xTe$, and $Cd_{1-x}Mn_xS$.

From a fundamental point of view, one of the most interesting and important aspects of DMS is the spin-glass (SG) state at low temperatures. In a SG the atomic magnetic moments are frozen into random directions due to random sites of the magnetic ions and frustrated interactions between the ions [4–6]. The SG transition temperature or freezing temperature T_f separates the SG and paramagnetic states. In bulk DMS materials T_f has been found to depend on the magnetic ion composition [7], the magnetic field [8], and the history of the system. Although some previous work has been devoted to the study of SG formation and dynamics in DMS [7, 8], the understanding of these processes is still far from complete [3].

With the drive towards miniaturization, physical properties of nanophase materials have remained an important and interesting subject for many years [9]. For semiconductors, such systems have been realized in quasi-2D systems of quantum wells (QWs), quasi-1D systems of quantum wires, and quasi-0D systems of quantum dots (QDs). Because of their unique electrical and optical properties, these nanostructures have great potential for revolutionary applications in nonlinear optics, fast optical switching devices, and memory devices. In a similar manner nanoscale magnetic particles have also shown useful, nonbulk behavior such as enhanced coercivities, magnetic moments, and altered Curie temperatures [10, 11].

In this paper we study a system which combines the themes above: the spin glass properties of ultrafine particles of the DMS $Cd_{1-x}Mn_xS$. There appears to be no previous work on the properties of SG materials in the ultrafine particulate form, i.e., zero-dimensional or quantum dot. On the other hand, two-dimensional thin film nanoscale SG systems have been studied in both DMS and metallic alloys. It was found that the SG freezing temperature T_f decreased with layer thickness; the transition survived down to monolayer thickness in the metallic alloys [12–15], whereas it disappeared in the DMS materials below some finite, nanoscale thickness [16]. It is therefore relevant to ask how T_f and other SG properties behave in zero-dimensional, ultrafine particles. Here we report data that show the SG properties of our nanoscale DMS differ in many ways from those of the bulk. We find that the SG freezing temperature decreases with particle size and seems to disappear below a critical size. We also find that the field dependence of T_f and the decay of the remanence magnetization are very different in the nanoparticle state.

2. Synthesis

$Cd_{1-x}Mn_xS$ nanoparticles were created by reacting Na_2S with a mixture of Mn^{2+} and Cd^{2+} ions in an aqueous solution at room temperature under argon. Aqueous solutions of Na_2S, $CdCl_2$, and $MnCl_2$ of molarity 0.25 M were prepared from $Na_2S \cdot 9H_2O$, 98% (Aldrich Chemical Co.) $CdCl_2$, 99 + % (Aldrich Chemical Co.), and $MnCl_2 \cdot 4H_2O$, 99.1% (Fisher Scientific). All compounds were ACS Reagent Grade. The water used in the preparation was distilled, deionized, and deoxygenated. The deoxygenation was accomplished by bubbling with argon gas.

Once the solutions were prepared, appropriate volumes of $MnCl_2$ and $CdCl_2$ were mixed in compliance with the Cd : Mn ratio desired in the final product of $Cd_{1-x}Mn_xS$. The pH of this solution was adjusted to be between 1.5 and 2.0 by adding HCl. This was necessary to avoid Mn hydroxide formation after the basic Na_2S solution was added. The aqueous solution of Na_2S was added last in accordance with the stoichiometry of the reaction,

$$(1-x)CdCl_2 + xMnCl_2 + Na_2S \rightarrow Cd_{1-x}Mn_xS + 2NaCl \quad (1)$$

to yield a yellow precipitate. The precipitate was sonicated for about 10 min in order to break large agglomerations of the precipitate. The precipitate was then washed several times with deoxygenated water, filtered, and placed in a desiccator (the desiccant used was $CaSO_4$) to dry under argon.

The dried precipitate was ground to a fine powder using an onyx mortar and a glass pestle. Portions of this were placed in Al_2O_3-coated tungsten boats and annealed under argon. The annealing temperatures ranged between 200 and 800°C. Each annealing was carried out for a period of $2\frac{1}{2}$ h, once

the target temperature was reached. The annealed sample was then allowed to cool slowly to room temperature over a period of several hours before removing it from the furnace for subsequent characterization.

3. Characterization

3.1. X-ray diffraction measurements

The mean crystal size, composition, and crystal structure were determined by X-ray powder analysis using a Scintag 2000 diffractometer operating with the Cu Kα line of wavelength 1.5406 Å. The angular range over which data was collected was between 20° and 60°. The system was calibrated using a strain-free SiO_2 crystal (Quartz) standard.

3.1.1. Structure

Fig. 1 presents the XRD spectra of nominally $Cd_{0.83}Mn_{0.17}S$ particles including the 'as-prepared' particles and four thermally annealed samples. For now, the composition variable x in $Cd_{1-x}Mn_xS$ is determined by the mixing stoichiometry in the reaction of Eq. (1). Included in Fig. 1 are also the standard line spectra of the bulk hexagonal and metastable structures of CdS and MnS provided by the JCPDS data base. By making comparisons with spectra obtained at different annealing temperatures, four features can be unambiguously identified. First, the XRD pattern clearly reveals that a single compound or alloy is formed since if CdS and MnS existed as two separate phases the MnS would give rise to a strong diffraction peak at 34.5° corresponding to its thermodynamically stable rock salt structure [17]. The absence of such a peak establishes the fact that a single alloy is formed. Second, the as-prepared particles have a cubic, zinc blende structure as indicated by a single peak in the angular region between 20° and 30° in conjunction with the absence of the (1 0 2) and (1 0 3) peaks at about 37° and 48°, respectively. Third, the single peak in the angular region between 20° and 30° evolves into a three peak pattern with increasing annealing temperature T_a, which, in conjunction with the appearance of the (1 0 2) and (1 0 3) peaks, indicates a change in the crystalline structure from the cubic, zinc blende structure to a hexagonal, wurtzite structure. This structural transition occurs at an annealing temperature of about 300°C. This transition has previously been observed to occur at a temperature near 300°C for CdS thin films prepared by chemical bath deposition [18]. Our previous work on CdX (X = S, Se, Te) ultrafine particles indicates a strong correlation between particle size and their structures [19]. Fourth, the XRD spectral line width decreases with increasing annealing temperature, indicating an increase in crystallite size with increasing T_a.

In order to understand the structural evolution of the particles with both temperature and composition, it is important to know the stable structures for the constituents. CdS which acts as the host in the DMS has a metastable cubic, zinc blende structure while its thermodynamic stable structure is the hexagonal, wurtzite structure [17]. MnS, on the other hand, has both zinc blende and wurtzite metastable structures while its thermodynamic stable structure is the cubic, rock salt structure [17, 20]. We find initially for the as-prepared sample that when these two materials combine to form the DMS alloy, the resulting structure emulates the structure of the host CdS, forming a metastable cubic phase. This is reasonable given the method by which the DMS particles are produced: rapid nucleation and growth from a supersaturated solution. The rapidity of similar precipitation reactions has been proposed to explain the creation of amorphous particulates of otherwise crystalline materials [21]. The cubic structure may result from its closer similarity to a roughly spherical nucleus, expected at the initial instant of nucleation, than the hexagonal structure [19]. If metastability is the proper explanation, then annealing will allow activation of the structure to the lower energy, stable, hexagonal structure [19]. This is clearly observed in Fig. 1, as well as in Fig. 2, where the XRD spectra of $Cd_{1-x}Mn_xS$ particles annealed at 500°C for different Mn concentrations are presented. Fig. 2 further reveals that the DMS alloy can be formed up to a limiting Mn concentration of $x \simeq 0.50$. Beyond this limit, in addition to the DMS alloy, MnS is formed and stays in its thermodynamically stable rock salt structure.

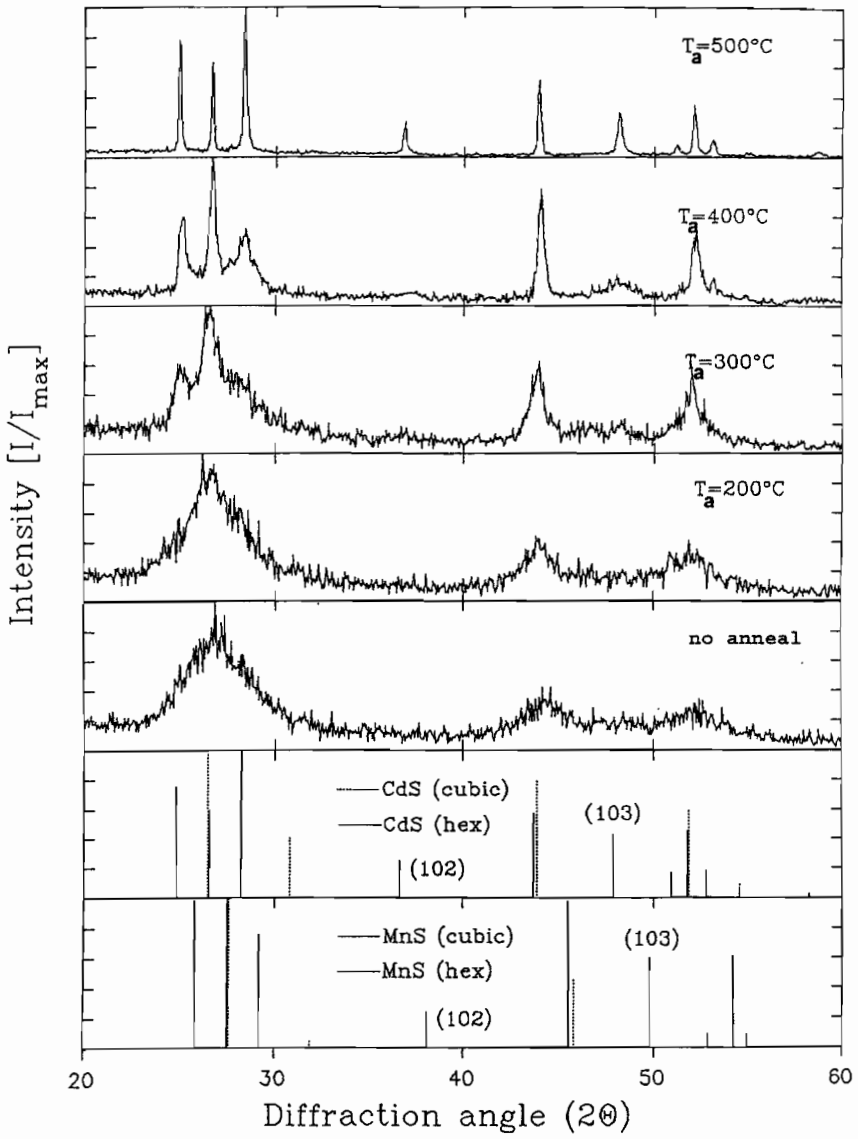

Fig. 1. X-ray diffraction spectra of the as-prepared and thermally annealed $Cd_{0.83}Mn_{0.17}S$ particles. Each annealing was carried out for a time of $2\frac{1}{2}$ h under argon. Also shown are the line spectra of the zinc blende and wurtzite structures of CdS and MnS.

3.1.2. Mean crystallite size

The mean crystallite diameter d was determined from the line width of the XRD spectra for different annealing temperatures by the Scherrer formula [22]

$$\langle d \rangle = \frac{0.94\lambda}{(B \cos \theta_B)}, \tag{2}$$

where λ is the X-ray wavelength, B is the full-width at half-maximum of the diffraction peak in units of radians, and θ_B is the half angle of the diffraction peak on the 2θ scale.

The results are shown in Table 1. The data clearly indicate that the crystallite size increases with increasing annealing temperature. The main source of error in our measurements was associated

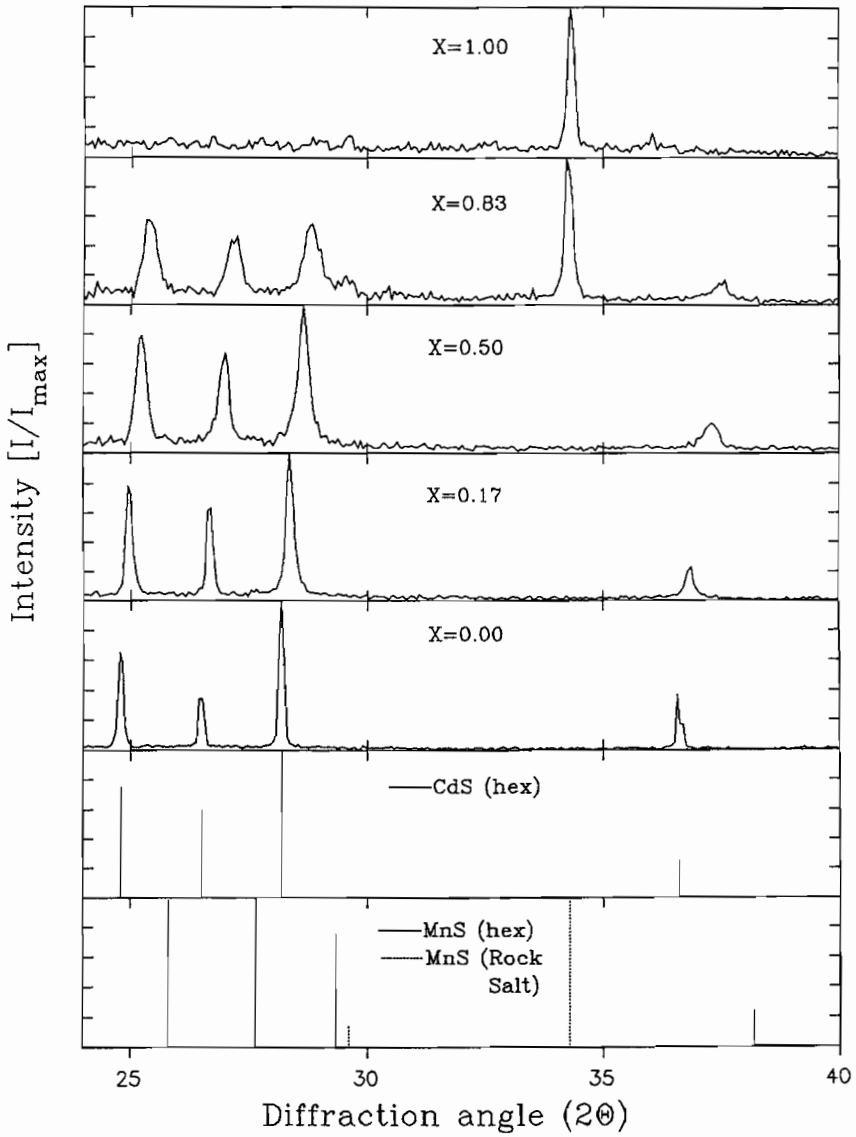

Fig. 2. X-ray diffraction spectra of $Cd_{1-x}Mn_xS$ particles with different Mn compositions annealed at 500°C for $2\frac{1}{2}$ h under argon. Also shown are the line spectra for the wurtzite structure of CdS and MnS as well as the cubic, rock salt structure for MnS.

with the intrinsic width of the diffractometer, which limits the measurable range to between 20 and 1200 Å.

3.1.3. Crystal composition

Apart from calculating the mean composition x of the alloy particles from the stoichiometry of the starting materials in solution during synthesis, a quantity we shall call x_{syn}, x could also be determined from the position of the XRD peaks, a quantity we shall call x_{XRD}. In Fig. 2 the two peaks at around 29° and 37° are the (1 0 1) and the (1 0 2) diffraction peaks, respectively. Both these peaks shift towards larger angles with increasing

Table 1
Mean crystallite size (in Å) of $Cd_{1-x}Mn_xS$ nanoparticles under different annealing temperatures T_a. The sizes were calculated using the Scherrer formula of Eq. (2) from the line width of the XRD peaks

T_a (°C)	$x = 0.00$	$x = 0.17$	$x = 0.30$	$x = 0.50$
24	27	25	25	24
200	33	30	26	24
300	93	95	71	74
400	270	250	210	160
450	—	—	—	345
500	910	635	570	500
550	—	—	—	610

Table 2
Diffraction angles for (1 0 1) and (1 0 2) XRD peaks of $Cd_{1-x}Mn_xS$ particles with different Mn compositions in the synthesis solution x_{syn}. Corresponding compositions, x_{XRD}, are calculated from the shift in the peaks. The last column gives x_{chem}, the Mn composition determined by chemical analysis of the particles.

x_{syn}	2θ (deg)		x_{XRD}		Average x_{XRD}	x_{chem}
	(1 0 1)	(1 0 2)	(1 0 1)	(1 0 2)		
0.00	28.16	36.60	0.00	0.00	0.00	—
0.17	28.32	36.90	0.16	0.20	0.18	0.17
0.30	—	—	—	—	0.28	—
0.50	28.66	37.36	0.50	0.52	0.51	0.51
0.83	28.82	37.58	0.66	0.65	0.66	—

x_{syn}. This was observed to be true for all peaks in the spectrum. Table 2 lists the diffraction angles for these two peaks which change from 28.16° to 28.82° and from 36.60° to 37.58°, respectively, corresponding to the increase in the synthesis composition x_{syn} from 0 to 0.83. Assuming a linear shift in the diffraction maxima with composition bounded by the pure phase maxima (Vegard's law [2]), the compositions can be calculated from the shifts of the (1 0 1) and (1 0 2) peaks, and are given both individually and averaged in Table 2. The data indicate that the compositions x_{syn} from the starting materials and x_{XRD} calculated from XRD measurements agree very well up to $x = 0.5$. For the case where $x_{syn} = 0.83$, the XRD shift data indicate a Mn composition of 0.65. Inspection of Fig. 2 shows a diffraction maxima at 34.50°, corresponding to the thermodynamically stable, rock salt structure of MnS (not indicated) implying an upper limit for the Mn composition [23].

As a further test of the value of x for our samples, the as-prepared samples of $Cd_{1-x}Mn_xS$ for $x = 0.17$ and $x = 0.5$ were sent for microanalysis to Galbraith Laboratories, Inc. Before analysis, the samples were dried for 2 h at a temperature of 120°C in a vacuum. Each sample was analyzed for Cd, Mn, and S. From the weight percentages determined by Galbraith the mole fractions for each element were calculated. These were then normalized to find the compositions x_{chem} which are also listed in Table 2. As can be seen, each of these measurements is in good agreement with the other two values of x, indicating that our synthetic technique is a success and also that our initial assumption of a linear shift in the XRD pattern is valid.

Finally, the consistency in composition values displayed in Table 2 reinforce our conclusion above that homogeneous compounds were formed and the consistency of Vegard's law indicates that the Mn^{2+} site distribution in the particles is the same as in the bulk.

3.2. Transmission electron microscopy measurements

TEM inspection was carried out using a Philips EM 201 electron microscope. The particles tend to cluster together making analysis of the cluster size difficult. Observation of $Cd_{1-x}Mn_xS$ samples annealed at different temperatures showed that the averaged particle size increased with annealing temperature consistent with XRD measurements.

4. Magnetic properties

A considerable amount of experimental and theoretical effort has been directed towards understanding the properties of SG materials [4–6]. In the broadest sense of the term a SG can be described as a collection of spins whose low-temperature state is a frozen-disordered one. A common feature of such a system is competition among the different interactions between the moments so that

no single configuration of spins is uniquely favored by all the interactions, a condition which is commonly known as frustration. Characteristic magnetic features of these SG systems are: the appearance of a sharp peak in the AC and DC susceptibilities at a temperature T_f, the freezing temperature below which the disordered spin-glass phase exists; the occurrence of irreversible behavior including remanence and coercivity below T_f; the presence of time and thermal-history-dependent magnetization below T_f; and a variety of other magnetic properties. Apart from bulk materials, SG properties have also been studied in layered quasi-2D systems (magnetic multilayers) and 2D DMS QWs and superlattices [2]. We know of no work on nanoparticle SG behavior. For these systems many of the physical properties are expected to change and become size-dependent.

For our $Cd_{1-x}Mn_xS$ DMS particles comparisons will be drawn between the particles and the corresponding bulk material. Since the samples annealed at 700°C and above showed line widths equal to the instrumental line width of the XRD (to imply sizes >1200 Å), these were considered to be bulk samples.

4.1. Composition dependence

Magnetic measurements were made with a SQUID magnetometer. The powdered samples had a mass of 10.0 mg and were contained in gelatin capsules. To find the spin-glass freezing temperature T_f the samples were zero-field-cooled (ZFC) to 1.7 K and then warmed slowly in an applied field of 100 G. A cusp in the magnetization measured in this way is an indication of a spin-glass transition.

In Fig. 3 we present data for the 'bulk' materials with compositions $x = 0.17$, 0.3, and 0.5 ($x = 0$ is diamagnetic and $x = 1$ is antiferromagnetic with a Néel temperature of 165 K). There is no cusp for $x = 0.17$, a small cusp below 5 K for $x = 0.3$, and a well-defined broad cusp at 17.5 ± 2.5 K for $x = 0.5$. Using high resolution in temperature scans for the $x = 0.3$ and 0.5 samples, T_f was measured to be 2.5 and 18 K, respectively. These data indicate a minimum composition for SG formation, consistent with the general behavior of all $A^{II}_{1-x}Mn_xB^{VI}$ DMS alloys where the minimum composition for

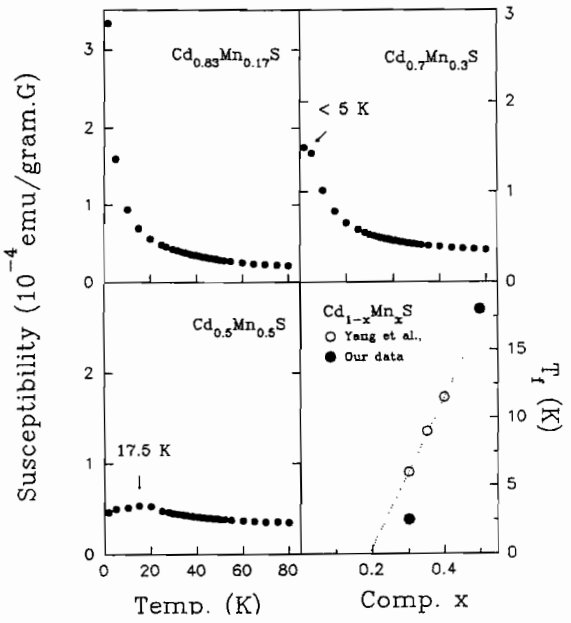

Fig. 3. ZFC susceptibility as a function of temperature for 'bulk' $Cd_{1-x}Mn_xS$ for three different Mn compositions $x = 0.17$, 0.3, and 0.5. The arrows indicate the position of the cusp which yields the SG transition temperature T_f. Lower right quadrant compares our data for T_f with previous results by Yang et al. [24] (dotted line) for bulk $Cd_{1-x}Mn_xS$ as a function of Mn composition, x.

SG formation in DMS bulk is believed to be $x \sim 0.2$ [2, 8]. Our results agree fairly well with previous studies on bulk $Cd_{1-x}Mn_xS$ DMS alloys by Yang et al. [24], as seen in the fourth quadrant of Fig. 3.

4.2. Size dependence

The size dependence of the SG freezing temperature T_f was investigated at a fixed magnetic ion composition of $x = 0.5$, which has the highest T_f (18 K) for the bulk material. Magnetization measurements under ZFC conditions revealed a SG transition temperature T_f that increased from $\sim$14–18 K with increasing particle size. Fig. 4 shows four representative plots of susceptibility vs. temperature for samples ranging from the as-prepared to the bulk for $Cd_{0.5}Mn_{0.5}S$.

An important observation obtained from these plots was the absence of a cusp for small particles

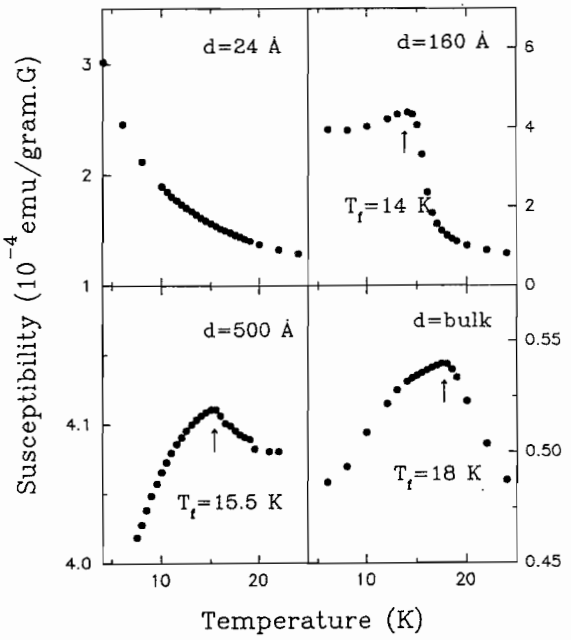

Fig. 4. Susceptibility of $Cd_{0.5}Mn_{0.5}S$ particles of different size. Data were taken while warming in a field of 100 G after ZFC. The transition temperature T_f is determined from the position of the cusp in these plots.

with a mean size of $d < 30$ Å [25]. This behavior implies that there may exist a critical size for SG formation in DMS nanoparticles. Such a critical size can be explained qualitatively by extending the SG empirical picture developed by Furdyna [2]. The picture rests on the insight obtained from neutron diffraction studies which revealed that antiferromagnetic interactions between neighboring spins in the DMS lead to formation of clusters of short-range order. The clusters grow in size with decreasing temperature. Hence, it would be reasonable to expect that a termperature will eventually be reached at which the cluster size is sufficiently large for correlated regions to 'touch'. This would result in clusters retaining their original identity, but having to interlock with each other, affecting their ability to respond to an external field. This interlocking process of different clusters is equated with the spin freezing temperature indicated by the cusp in the magnetic susceptibility. For particles one can infer that in order to observe a SG transition the particle size has to be sufficiently large for the correlated regions to touch and interlock with each other. If the size of the correlated regions become comparable to or larger than the particle size, then only one cluster will exist inside the particle and there can be no SG transition. Hence, there is a critical size for SG formation.

Previous work on finite size effects on the T_f of SG systems involved both the classical metallic systems of Cu : Mn and Ag : Mn [12–15] and a DMS material, $Cd_{1-x}Mn_xTe$ [16]. All were layered, quasi-two-dimensional systems. Fig. 5 shows the depression in the relative SG freezing temperature, $T_f(d)/T_f(\infty)$, vs. d for our system and includes lines which represent the average trend of the data from the metallic systems. Remarkably, the $T_f(d)/T_f(\infty)$ that we see is roughly the same as that observed in the metallic layered systems when

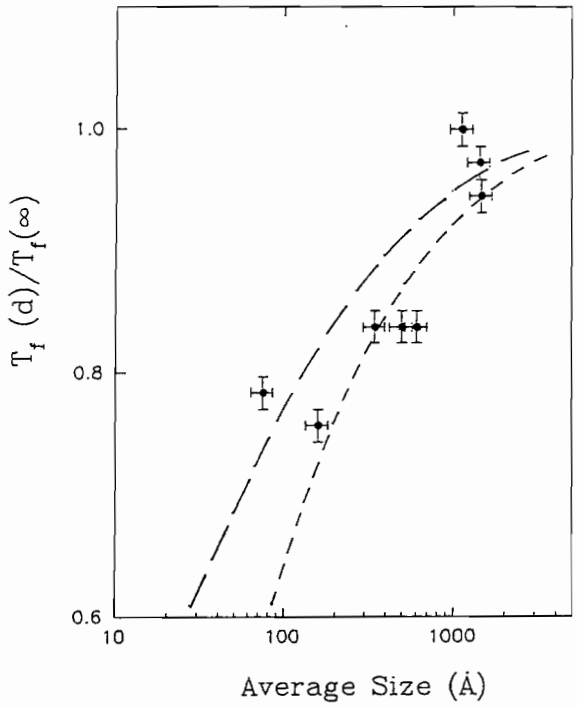

Fig. 5. Spin-glass freezing temperature relative to the bulk as a function of particle mean size for $Cd_{0.5}Mn_{0.5}S$. The short and long dashed lines represent the average dependence on layer thickness observed in metallic SG systems from Refs. [13, 15], respectively.

plotted versus layer thickness over our limited range of $T_f(d)/T_f(\infty)$.

The behavior of our smallest size, however, is significantly different than the thinnest metallic systems in that no SG transition is seen in our system. The careful work of Hoines et al. [15] established that the SG transition persists down to monolayer thickness for 2D, metallic systems. It is possible that a transition exists below 1.7 K in our systems, but the rough similarity in Fig. 5 implies that for $d = 24$ Å we should find $T_f \sim 5 \pm 2$ K. Awschalom et al. [16] saw the cusp in χ vs. T disappear for their thinnest, 20 Å layers of the DMS $Cd_{1-x}Mn_xTe$, which corroborates our result. However, unlike our result, no shift in the cusp was seen as a function of size (layer thickness). Thus, the experimental situation is unclear. We conclude that for our DMS, 0D particles a depression in T_f is seen with declining size which is initially similar to that seen in metallic, 2D systems. However, unlike these systems our smallest size shows no SG transition. The lack of a transition could be due to the cubic structure of these smallest particles, but this seems unlikely because the cation nearest-neighbor distribution is the same for both the hexagonal and cubic phases. Another reason for the different $d \to 0$ behavior could be the different magnetic coupling, which is ferromagnetic and long ranged in the metallic systems and antiferromagnetic short ranged in the DMS system. Basing the difference on the different materials is supported by the Awschalom et al. result, if one ignores their lack of size dependence. Finally, the different behavior could be due to the different dimensionality, 0D vs. 2D, an explanation which, given the data available, has no inconsistencies.

4.3. Field dependence

Figs. 6 and 7 show susceptibility versus temperature 'cusps' for $Cd_{0.5}Mn_{0.5}S$ at different applied fields for $d = 345$ Å and bulk, respectively. The temperatures at which these peaks occur are the SG freezing temperatures T_f and are plotted in Fig. 8 as a function of field. A remarkable difference in behavior is seen between the particulate and bulk data. The bulk behavior is similar to previous experiments [2, 6, 26, 27] in three ways. First, T_f declines with field H in a manner similar to that predicted by theory described by

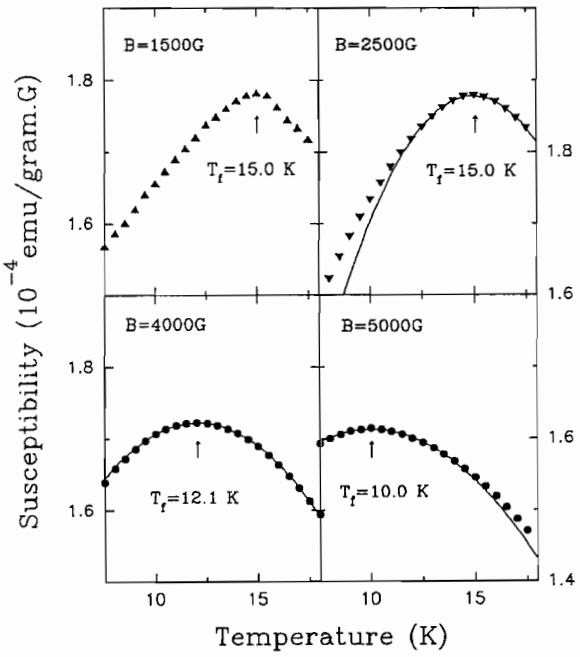

Fig. 6. ZFC susceptibility vs. temperature for $Cd_{0.5}Mn_{0.5}S$ particles with a diameter of 345 Å measured in different fields.

$$T_f(B) = T_f(0)\,(1 - \alpha_b\, B^{2/3}). \tag{3}$$

The curve fitting the data for the bulk $Cd_{0.5}Mn_{0.5}S$ (open squares) is the least-squares fit to Eq. (3). The fitted values are $T_f(0) = 17.3$ K and $\alpha_b = 7.45 \times 10^{-4}\,G^{-2/3}$. Second, the magnitude of the decrease is significantly greater [26, 28] than that predicted by theory [29–31] as indicated by the large value of α_b compared to the expected values of $\alpha \simeq 10^{-5}$–$10^{-4}\,G^{-2/3}$. Third, the data indicate that the peak profile of the plots tends to flatten out with increasing applied field. This behavior may be attributed to small local fluctuations of the composition around the nominal value of x in the sintered samples [24]. In striking contrast is the behavior for the particles which show no field dependence for small field, yet a stronger and fairly linear, over the limited range, dependence above a large threshold field of 2.6 kG. This behavior can

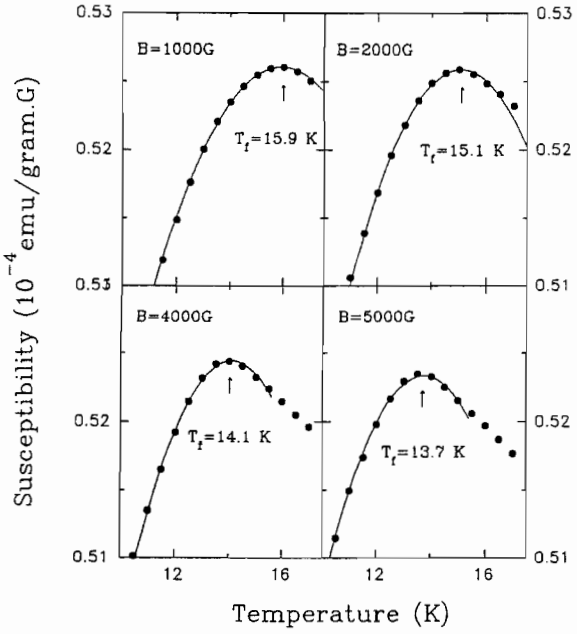

Fig. 7. ZFC susceptibility vs. temperature for bulk $Cd_{0.5}Mn_{0.5}S$ measured in different fields.

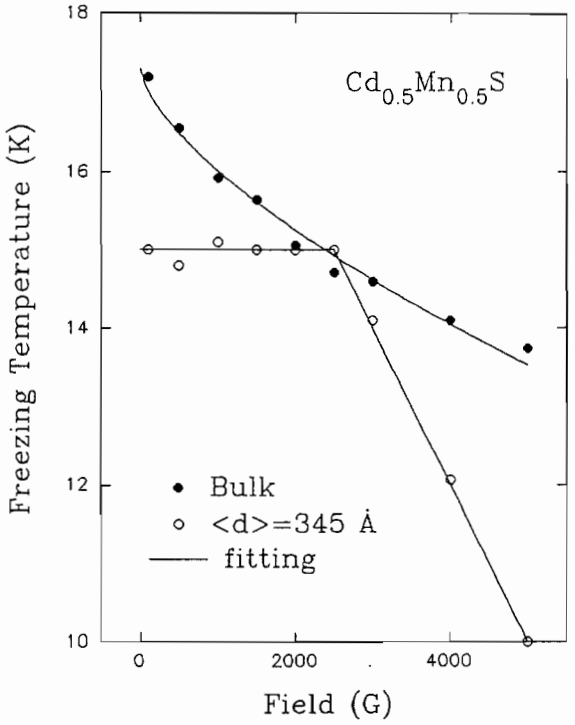

Fig. 8. Magnetic field dependence of the SG transition temperature T_f for $Cd_{0.5}Mn_{0.5}S$ particles of size $d = 345$ Å (open circles) and for the bulk (filled circles).

be described by

$$T_f(B) = \begin{cases} T_f(0), & B < B_0, \\ T_f(0)[1 - \alpha_p(B - B_0)], & B > B_0. \end{cases} \quad (4)$$

The curve through the data for the particulate $Cd_{0.5}Mn_{0.5}S$ (solid circles) is the least-squares fit to Eq. (4). Fit values are $T_f(0) = 14.9$ K, $\alpha_p = 2.0 \times 10^{-3}$ G^{-1} and $B_0 = 2.6$ kG. A clue to understanding this result may lie in the fact, see below, that the coercivity of the particles is 1.5 kG, close to the threshold field. It is well known that small particles have enhanced coercivities often due to surface anisotropies [11, 32], and that the nature of the SG phase diagram in T–B space is sensitive to magnetic anisotropies.

4.4. Relaxation of remanent magnetization

One of the characteristic features of a SG system is the presence of a history and time-dependent remanent magnetization below the freezing temperature T_f. Here we study the isothermal remanent magnetization (IRM). The measurements were made for $Cd_{0.5}Mn_{0.5}S$ particles of size 74 Å and the bulk material.

4.4.1. Field dependence

IRM relaxations were measured with the samples ZFC from 300 to 10 K. An external field ranging from 1000 to 6000 G was applied for 300 s before being turned off and a small measuring field of 10 G was applied. The upper and lower left quadrants in Fig. 9 show IRM relaxations of $Cd_{0.5}Mn_{0.5}S$ particles ($d = 74$ Å) and the bulk material for three applied fields of 2, 4, and 6 kG, respectively. The data were fit using least squares to

$$\sigma(t) = \sigma_0 t^{-\alpha} \quad (t > t_0, t_0 = 45 \text{ s}), \quad (5)$$

where α is the decay exponent. Eq. (5) is typical for SG relaxation [1, 4, 33]. The adjacent two quadrants in Fig. 9 (the upper and lower right), feature

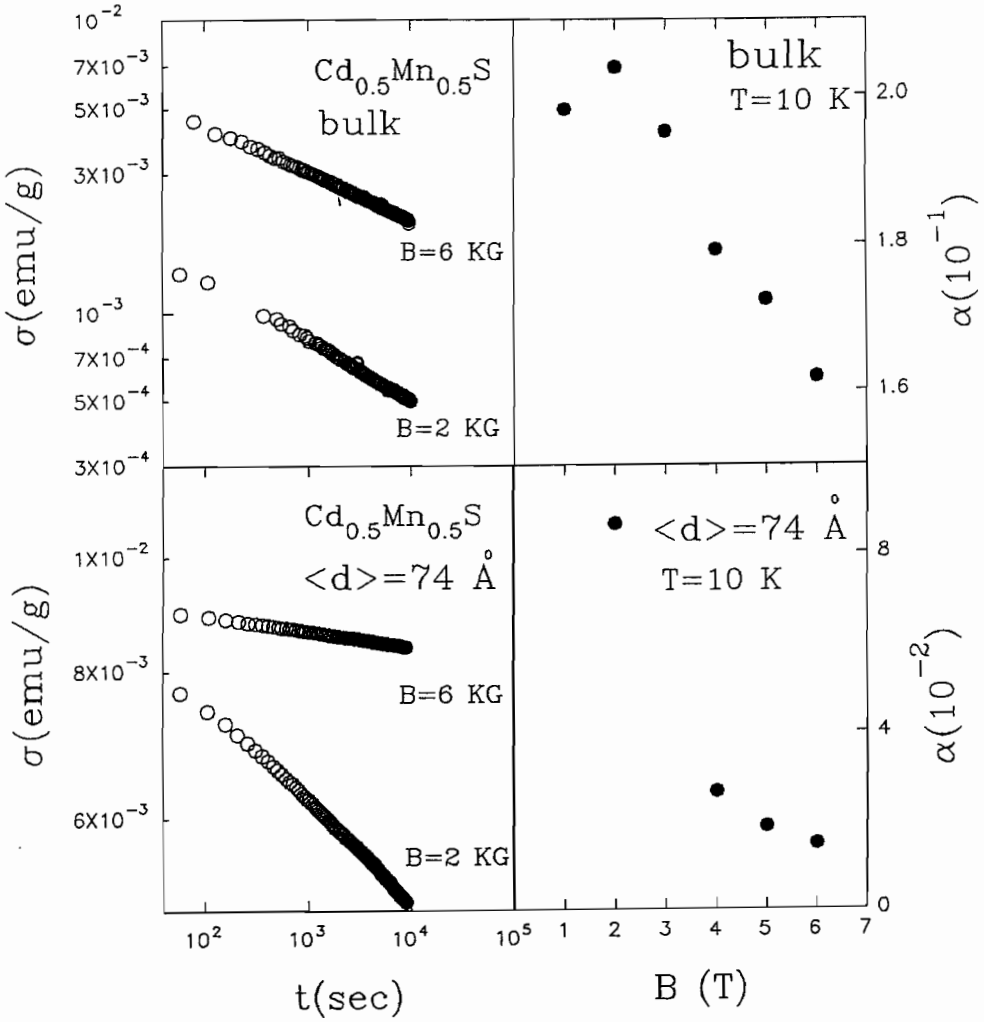

Fig. 9. Field dependence of the IRM relaxations in $Cd_{0.5}Mn_{0.5}S$ particles with a diameter of 74 Å and the bulk material. The upper and lower quadrants on the left show our data for the particles and the bulk material, respectively. In the two quadrants on the right the decay exponent α is plotted as a function of applied field.

the decay exponent α as a function of applied field for each material.

Fig. 9 shows that the IRM relaxation of both the particles and the bulk material can be described by a power-law decay given by Eq. (5). The decay exponent α for both materials decreases with increasing applied field. This is consistent with previous reports on $Cd_{1-x}Mn_xTe$ DMS bulk materials [33]. However, the decay exponent α for the particles is as much as an order of magnitude smaller than for the bulk, indicating a much slower decay rate, and it has a much stronger dependence on field. The σ_0 for the particles is nearly two orders of magnitude larger than that for the bulk. One possible interpretation is that the particle's IRM is the sum of the small, quickly decaying IRM of the bulk plus a large, constant background remanence due to the particulate nature. This scenario is not viable, however, because attempts to subtract a background from the particle IRM led to curved log–log plots, i.e., nonpower-law decays.

4.4.2. Temperature dependence

The temperature dependence on IRM relaxation was measured with the applied magnetic field fixed at 5 kG. The samples were ZFC to the desired temperature, which ranged between 5 and 15 K, and the external field of 5 kG was then applied for 300 s before a small measuring field of 10 G was applied. As before, the two quadrants on the left in Fig. 10 show the IRM relaxations of $Cd_{0.5}Mn_{0.5}S$ particles ($d = 74$ Å) (above), and the bulk (below) for three representative temperatures each. The data have been fit to Eq. (5). The adjacent two quadrants in Fig. 10 (the upper and lower right) show the decay exponent α as a function of temperature for each material.

As in the previous case, we see that the power law given by Eq. (5) can be used to describe the relaxation in both materials. The decay exponent α decreases with increasing temperature, and is approximately four times smaller for the particles than for the bulk material.

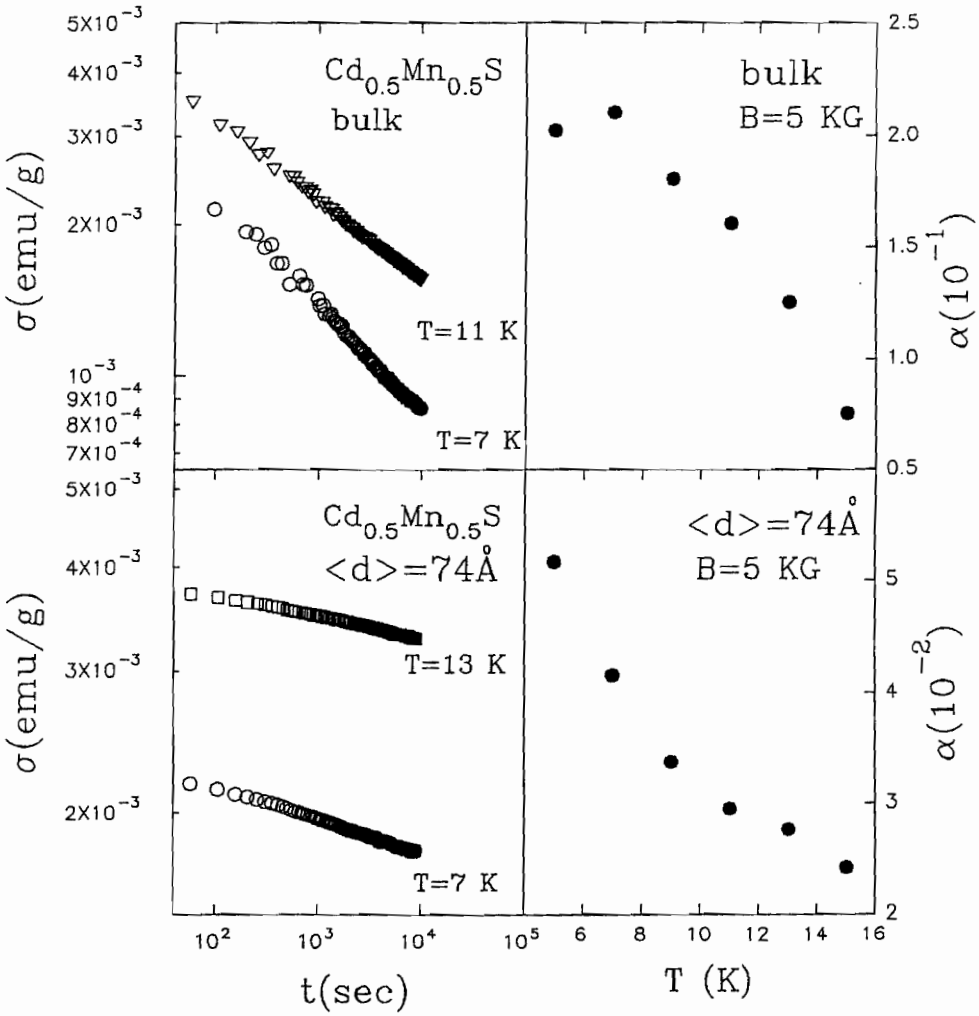

Fig. 10. Temperature dependence of the IRM relaxations in $Cd_{0.5}Mn_{0.5}S$ particles with a diameter of 74 Å and the bulk material. The upper and lower quadrants on the left show our data for the particles and the bulk material, respectively. In the two quadrants on the right the decay exponent α is plotted as a function of temperature.

4.5. Hysteresis measurements

Magnetic properties were further investigated for $Cd_{0.5}Mn_{0.5}S$ DMS particles and the bulk material by measuring the coercivity and remanence from hysteresis loops. Fig. 11 shows part of the hysteresis loops of the as-prepared sample measured at three different temperatures. At $T = 35$ K, the magnetization is saturated at about 3.5 kG, whereas at $T = 4.5$ K saturation is reached only at fields in excess of 15 kG. In order to make comparisons between the particles and the corresponding bulk material, part of a hysteresis loop for bulk $Cd_{0.5}Mn_{0.5}S$ is also included in Fig. 11 (inset). Fig. 11 shows a coercivity for the $Cd_{0.5}Mn_{0.5}S$ DMS particles at $T = 4.5$ K to be about 3.5 kG which is about one order of magnitude larger than the coercivity of the bulk material (about 0.3 kG) measured at the same temperature. The figure also shows that the remanence of magnetization in the particles depends strongly on temperature and is reduced by a factor of two when the temperature increases from 4.5 to 35 K. Furthermore, the remanence of magnetization in $Cd_{0.5}Mn_{0.5}S$ particles compared with its bulk material is more than one order of magnitude larger.

Hysteresis measurements were also made for $Cd_{0.5}Mn_{0.5}S$ particles of different sizes. Our measurements indicate that both coercivity and remanence decrease with the increase of temperature and the particle's size. The enhancements in remanence and coercivity in particles may be related to the surface pinning of the magnetic moments [34].

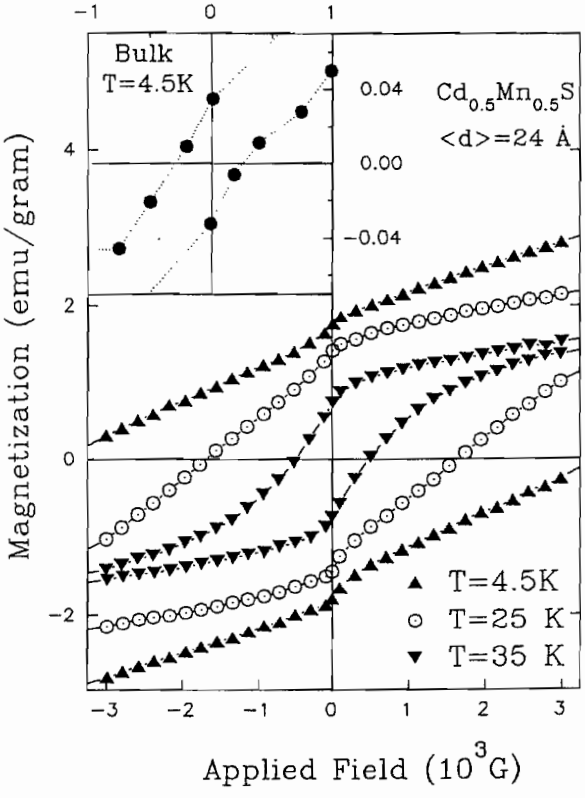

Fig. 11. Partial hysteresis loops of the as-prepared $Cd_{0.5}Mn_{0.5}S$ particles at three different temperatures. The inset shows a partial hysteresis loop of the bulk material taken at $T = 4.5$ K.

5. Conclusions

$Cd_{1-x}Mn_xS$ DMS ultrafine particles have been chemically synthesized using aqueous solution precipitation and subsequent heat treatment for compositions x from 0 to 0.50 and sizes ranging from approximately 20 Å to the bulk. The as-prepared particles had sizes between 20 and 30 Å and had the cubic, zinc blende structure. The appearance of this metastable structure may be attributed to the rapid nucleation and growth from the supersaturated solution. Thermal annealing under an Ar atmosphere increased the particle size and changed its structure to the stable, hexagonal, wurtzite form.

The spin-glass magnetic properties of the particles were significantly different than the bulk. The SG freezing temperature decreased with decreasing particle size and could not be observed in the smallest particles with $d \simeq 20$ Å. The SG freezing temperature for the particles was independent of the applied field, unlike the bulk behavior, but then developed a strong dependence above a field comparable to the rather large coercivity. The remanent magnetization was also significantly larger than the bulk, decreased with increasing particle size and decayed with a power law in time, as the bulk does, but with much smaller exponent. The SG freezing temperature and remanent magnetization behavior of the particles point to the surface of the particles

as the source of the deviations from bulk behavior. At the surface both uncompensated spins and additional spin pinning, i.e., surface anisotropy, can and apparently do occur as indicated by the hysteresis behavior.

Acknowledgements

The authors would like to thank professors M. O'Shea and G. Wysin for helpful discussion, and M. Smith, J.Z. Li, J.P. Chen, P. Perera, and G.W. Wen for experimental insights. This work is supported by NSF grant OSR 92-55223.

References

[1] J.K. Furdyna and J. Kossut, in: Semiconductors and Semimetals, Vol. 25 (Academic Press, New York, 1988).
[2] J.K. Furdyna, J. Appl. Phys. 64 (1988) R29.
[3] M. Smith, A. Dissanayake and H.X. Jiang, Phys. Rev. B 49 (1994) 4514.
[4] D. Chowdhury, Spin Glasses and Other Frustrated Systems (World Scientific, Singapore, 1986).
[5] K.H. Fischer and J.A. Hertz, Spin Glasses (University Press, Cambridge, 1991).
[6] J.A. Mydosh, Spin Glasses: An Experimental Introduction (Taylor and Francis, London, 1993).
[7] R.R. Galazka, S. Nagata and P.H. Keesom, Phys. Rev. B 22 (1980) 3344.
[8] S.B. Oseroff, Phys. Rev. B 25 (1982) 6584.
[9] M. Reed and K. Kirk, in: Nanostructure and Mesoscopic Systems (Academic, San Diego, 1991).
[10] G.C. Hadjipanayis and R.W. Seigle, in: Nanophase Materials (Kluwer, The Netherlands, 1994).
[11] S. Gangopadhyay, G.C. Hadjipanayis, B. Dale, C.M. Sorensen, K.J. Klabunde, V. Papaefthymiou and A. Kostikas, Phys. Rev. B 45 (1992) 9778.
[12] G.G. Kenning, J.M. Slaughter and J.A. Cowen, Phys. Rev. Lett. 59 (1987) 2596.
[13] A. Gavrin, J.R. Childress, C.L. Chien, B. Martinez and M.B. Salamon, Phys. Rev. Lett. 64 (1990) 2438.
[14] G.G. Kenning, J. Bass, W.P. Pratt, Jr., D. Leslie-Pelecky, L. Hoines, W. Leach, M.L. Wilson, R. Stubi and J.A. Cowen, Phys. Rev. B 42 (1990) 2393.
[15] L. Hoines, R. Stubi, R. Loloee, J.A. Cowen and J. Bass, Phys. Rev. Lett. 66 (1991) 1224.
[16] D.D. Awschalom, J.M. Hong, L.L. Chang and G. Grinstein, Phys. Rev. Lett. 59 (1987) 1733.
[17] T.C. Bailar, Jr., H.J. Emeleus, R. Nyholm and A.F. Trotman-Dickenson, Comprehensive Inorganic Chemistry (Elmsford, New York, 1973).
[18] O. Zelaya-Angel, J.J. Alverado-Gil, R. Lozada-Morales, H. Vargas and A.F. da Silva, Appl. Phys. Lett. 64 (1994) 291.
[19] R.J. Bandaranayake, G.W. Wen, J.Y. Lin, H.X. Jiang and C.M. Sorensen, Appl. Phys. Lett. 67 (1995) 831.
[20] G. Nickless, Inorganic Sulphur Chemistry (Elsevier, Amsterdam, 1968).
[21] J. Van Wonterghem, S. Morup, C.J.W. Koch, S.W. Charles and S. Wells, Nature 322 (1986) 622.
[22] B.D. Cullity, Elements of X-ray Diffraction (Addison-Wesley, Reading, MA, 1978).
[23] R.J. Bandaranayake, M. Smith, J.Y. Lin, H.X. Jiang and C.M. Sorensen, IEEE Trans. Magn. 30 (1994) 4930.
[24] Y.Q. Yang, P.H. Keesom, J.K. Furdyna and W. Giriat, J. Solid State Chem. 49 (1983) 20.
[25] R.J. Bandaranayake, J.Y. Lin, H.X. Jiang and C.M. Sorensen, IEEE Trans. Magn. 31 (1995) 3761.
[26] G.G. Kenning, D. Chu and R. Orbach, Phys. Rev. Lett. 66 (1991) 2923.
[27] S. Oseroff and P.H. Keesom, in: Semiconductors and Semimetals, Vol. 25 (Academic Press, New York, 1988).
[28] R.V. Chamberlin, M. Hardiman, L.A. Turkevich and R Orbach, Phys. Rev. B 25 (1982) 6720.
[29] G. Toulouse and M. Gabay, J. Phys. (Paris) Lett. 42 (1981 L013.
[30] J.R.L. d'Almeida and D.J. Thouless, J. Phys. A 11 (1978 983.
[31] K.H. Fischer, Z. Phys. B 60 (1985) 151.
[32] F. Bodrer, S. Morup and S. Linderoth, Phys. Rev. Lett. 7 (1994) 282.
[33] S. Oseroff and F.G. Gandra, J. Appl. Phys. 57 (1985) 3421
[34] F. Bodker, S. Morup and S. Linderoth, Phys. Rev. Lett. 7 (1994) 282.